

10

15

20



MIPV-NWP-PINN V1.0: Development of a Multi-scale Photovoltaic Power Forecasting Framework Integrating Numerical Weather Prediction with Physics-Informed Neural Networks

Fei Zhang^{1,2,3}, Xingcai Li¹, Zifa Wang^{2,3,4}, Yunyun Wen¹, Xuyang Zhou¹, Zichen Wu^{2,3,4}, Zhuoran Wang^{2,3,4}, Huansheng Chen^{2,3,4}, Zhe Wang^{2,3,4}, Xueshun Chen^{2,3,4}

¹School of Physics, Ningxia University, Yinchuan, 750021, China

²State Key Laboratory of Atmospheric Environment and Extreme Meteorology (AEEM), Institute of Atmospheric Physics, Chinese Academy of Sciences, Beijing 100029, China

³Key Laboratory of Atmospheric Boundary Layer Physics and Atmospheric Chemistry (LAPC), Institute of Atmospheric Physics, Chinese Academy of Sciences, Beijing 100029, China

⁴College of Earth and Planetary Sciences, University of Chinese Academy of Sciences, Beijing 100049, China

Correspondence: Xingcai Li (nxulixc2011@126.com) and Xueshun Chen (chenxsh@mail.iap.ac.cn)

Abstract: Photovoltaic (PV) power generation has become a cornerstone of clean energy, for which accurate forecasting is essential to ensure safe and efficient grid integration. However, raw Numerical Weather Prediction (NWP) outputs often fail to provide reliable forecasts because PV power is influenced by multiple coupled factors, including meteorological factors and photovoltaic modules. To address this challenge, this study develops a multi-scale PV power forecasting framework that integrates NWP with deep learning techniques (MIPV-NWP-PINN) and evaluates its performance using PV module monitoring data from a power station in northwestern China. First, a regional high-resolution NWP system based on the Weather Research and Forecasting (WRF) model is established to generate multi-scale meteorological forecasts with lead times of 6 hours, 1 day, 3 days, and 5 days. Next, a novel hybrid correction model that combines Quantile Mapping with a Temporal Pattern Attention-based Long Short-Term Memory (TPA-LSTM) network is proposed to improve the accuracy of Global Horizontal Irradiance (GHI) forecasts. This correction approach reduces the Mean Absolute Error (MAE) and Root Mean Squared Error (RMSE) by more than 23% compared to raw NWP outputs. Building on these corrected meteorological forecasts, a Physics-Informed Neural Network (PINN)-iTransformer model is developed for the final prediction of PV power. By incorporating physical constraints directly into its loss function, this model consistently outperforms state-of-the-art alternatives across all forecasting horizons, achieving reductions of 15.5% in RMSE and 12.4% in MAE. This physicsconstrained framework substantially improves the accuracy and robustness of PV power forecasting across multiple time scales. The enhanced reliability directly supports secure PV grid integration and contributes to the broader transition toward lowcarbon energy systems.

1 Introduction

30

The rapid expansion of Photovoltaic (PV) power is reshaping the global energy landscape; it is projected to become the dominant renewable energy source by 2029 and is expected to constitute 8.3% of the total electricity supply by 2025 (Iea,

1

https://doi.org/10.5194/egusphere-2025-4439 Preprint. Discussion started: 28 October 2025 © Author(s) 2025. CC BY 4.0 License.



45

50

55

60



2024). Within this context, Northwest China, due to its abundant solar resources, has become a key region for the global PV industry's growth. The region's high solar irradiance and clear-sky index provide ideal conditions for large-scale, centralized PV plants, establishing it as the primary area for such deployments in China. However, the challenge of accurate PV forecasting is magnified in this region, which is characterized by an arid desert climate and complex meteorological dynamics. This environment is not only susceptible to frequent extreme weather, such as dust storms, but also experiences significant attenuation and variability in Global Horizontal Irradiance (GHI) due to high concentrations of anthropogenic aerosols (Nie and Mao, 2021). These uncertainties significantly impair the performance efficiency of PV modules and introduce substantial challenges to power grid stability and operational security. Consequently, accurate GHI forecasting is essential for ensuring the economic viability of power stations and maintaining the stability of the energy system.

Many PV power forecasting studies inflate model performance by using actual weather data as input, a practice that does not reflect real-world forecasting scenarios (Dai et al., 2025). High-precision meteorological forecasts are crucial for enhancing the accuracy of PV power predictions, particularly for physics-based models (Das et al., 2018; Dai et al., 2025). While Numerical Weather Prediction (NWP) provides such forecasts, its outputs often exhibit significant deviations from actual observations. Therefore, improving the accuracy of NWP-derived GHI has become a key challenge in the operation of PV systems. Literature consensus suggests that mainstream radiation transfer schemes, like those in the Weather Research and Forecasting (WRF) model, systematically overestimate GHI across various weather conditions. This bias is amplified by increasing cloud cover and aerosol influence (Zempila et al., 2016). To mitigate this bias, researchers have incorporated factors such as aerosols into their models (Ruiz-Arias et al., 2014). Despite these efforts, models still fail to overcome the GHI overestimation problem. For instance, Yue et al. (2025) demonstrated that WRF-Solar tends to underestimate total cloud fraction in China, leading to a persistent overestimation of GHI. This issue becomes particularly acute in China's arid and semi-arid regions, where most large-scale PV plants are clustered. In these areas, the complex mixture of dust and anthropogenic aerosols, compounded by the NWP model's deficiencies in representing cloud microphysics, further amplifies forecast uncertainty.

Given the complexity and expense of directly modifying the core of NWP models, statistical post-processing techniques have emerged as a cost-effective alternative. For instance, Visaga et al. (2024) employed a Kalman filter (KF) to post-process WRF-generated GHI, reducing its Root Mean Squared Error (RMSE) by 17%. Similarly, Khan and Jama (2024) implemented bias correction using a nonlinear regression model, while Rincón et al. (2018) combined KF with model output statistics, achieving up to a 97% reduction in annual GHI bias compared to raw forecasts. Alvarenga et al. (2022) used an Artificial Neural Network (ANN)-KF model for GHI correction, reducing the Mean Absolute Error (MAE) of the raw GHI by 45%. These studies demonstrate that statistical post-processing is a powerful tool for improving NWP forecast accuracy at a modest computational cost. Therefore, applying bias correction to NWP outputs is a proven strategy for enhancing the practical utility of PV power

https://doi.org/10.5194/egusphere-2025-4439 Preprint. Discussion started: 28 October 2025 © Author(s) 2025. CC BY 4.0 License.



65

70

75

80

85

90



forecasts. Despite these advances, significant opportunities remain for developing more sophisticated statistical correction algorithms to further improve the reliability of forecasts.

Furthermore, even a corrected irradiance forecast is not the final product; a subsequent modeling step is required to convert this meteorological data into a PV power prediction. The methods to solve this problem are broadly classified into three categories: physical, data-driven, and hybrid models (Gupta et al., 2025; Li et al., 2025). Physical models, exemplified by the five-parameter model, simulate power output from the intrinsic parameters of PV modules (De Soto et al., 2006), but their practical performance is often limited (Wang et al., 2019). In contrast, data-driven statistical methods have become the mainstream approach due to their flexibility and high accuracy. Traditional statistical models, including Multiple Linear Regression (Alskaif et al., 2020), Random Forest (Kumar et al., 2025), and Support Vector Machine (Vandeventer et al., 2019), have been increasingly superseded by deep learning architectures. For example, Multi-Layer Perceptron (MLP) (Liu and Gai, 2025), Recurrent Neural Network (Vu and Chung, 2022), Long Short-Term Memory (LSTM) (Guo et al., 2025; Liu et al., 2024), and Transformer (Piantadosi et al., 2024; Wu et al., 2024a) have been applied to prediction owing to their superior non-linear feature extraction capabilities. Predictive accuracy can be refined through hybrid frameworks, often employing metaheuristic algorithms for hyperparameter optimization (Zhai et al., 2025; Peng et al., 2024). Nevertheless, purely data-driven models are inherently 'black-box' in nature. Their prediction process lacks physical interpretability and even yields outputs that violate fundamental physical laws in scenarios with sparse or noisy training data.

Hybrid models that fuse physical principles with statistical learning have emerged to address limitations in PV power forecasting. These frameworks range from mechanism-driven hybrids to statistical-physical fusion models (Santos et al., 2024). A common strategy involves a 'shallow' or sequential integration of physics. For instance, the Physical-Hybrid Artificial Neural Network (PHANN) couples a solar radiation model with MLP (Dolara et al., 2015; Hottel, 1976). Other works have adopted similar cascaded structures, such as using a physical model to compute module-surface irradiance as an input feature for an LSTM network (Wu et al., 2024b), or to establish a baseline physics prediction that an ANN subsequently refines to capture residual dynamics (Zhang et al., 2024). Despite improving accuracy, these cascaded frameworks lack deep mechanistic integration. In contrast, Physics-Informed Neural Networks (PINN) provide a more profound mechanistic basis. PINN embeds physical laws, often in the form of differential equations, directly into the neural network's loss function, compelling the model to adhere to physical principles during training (Raissi et al., 2019). Although PINN has been applied to related PV tasks, such as temperature prediction (Wang et al., 2025), its direct application to PV power forecasting remains underexplored. Deeply coupling PINN with advanced time-series models for direct PV power prediction represents a significant, yet largely untapped, research area with substantial scientific merit.

To bridge these research gaps, this study develops a NWP-driven multi-scale photovoltaic forecasting framework that fundamentally integrates physical principles with data-driven modeling through deep synergistic coupling (MIPV-NWP-



100

105

110

115



PINN). The MIPV-NWP-PINN comprises a hierarchical, multi-module forecasting chain, with its technical pipeline illustrated in Figure 1. Firstly, we establish a WRF prediction system to generate fine-grained numerical weather forecasts. Secondly, we design a hybrid correction module employing a Quantile Mapping -Temporal Pattern Attention-Long Short-Term Memory (QM-TPA-LSTM) network to enhance the GHI accuracy. Following this, a physical model is utilized to calculate the plane-of-array irradiance (G_{POA}). For the final task of PV power prediction, we construct a PINN-iTransformer model by incorporating the physical equations constraint. This 'physics-constrained, data-driven' hybrid architecture excels in statistical performance and significantly improves physical consistency and interpretability. This paper is structured as follows: Section 1 provides an introduction to the core issues and scope of the study. Section 2 presents the theoretical underpinnings and methodologies employed. Section 3 elaborates on the process of GHI correction and estimation. Finally, Section 4 details the PV power prediction, including a comparative analysis against other established models.

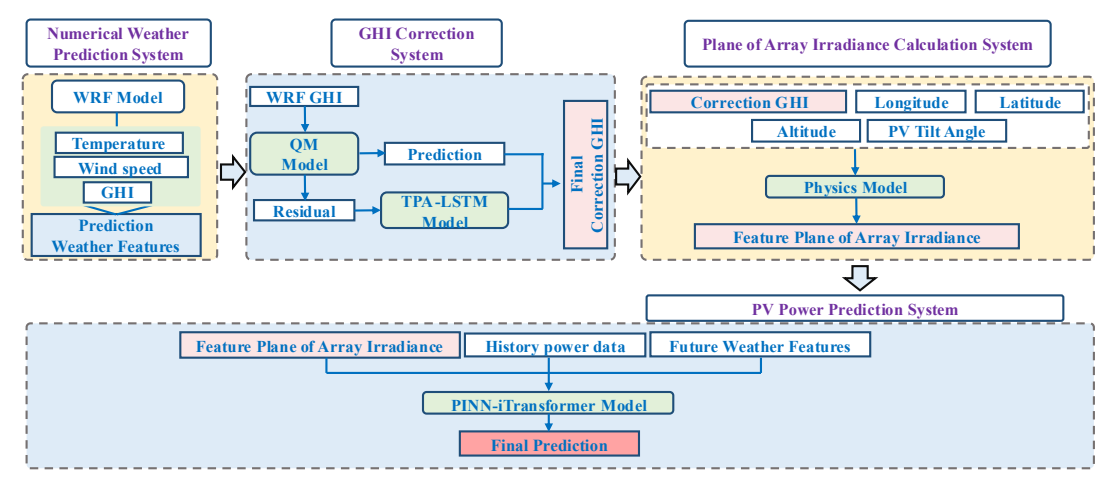


Figure 1: Flowchart of the MIPV-NWP-PINN.

2 Data and Methods

2.1Data Acquisition

The proposed forecasting framework was empirically evaluated using high-resolution data from a PV power station in Zhongwei, Ningxia, China (37.53°N, 105.04°E), as depicted in Figure 2(c). The system recorded key variables including ambient air temperature, GHI, wind speed, wind direction, PV module temperature, and PV power output. Data were collected from June 1 to July 31, 2020, with a temporal resolution of 120 seconds. This observational dataset calibrated and evaluated all NWP simulations and subsequent power forecasting models. The technical specifications and related parameters of the sampling equipment are detailed in Table S1(in the support file). We incorporated GHI data from six additional National Solar Radiation Database (NSRDB) stations to assess the framework's spatial generalizability. The GHI data from these stations are well-established to exhibit high agreement with ground-based measurements (Sengupta et al., 2018). The geographical



125

130

135

140



distribution of these six stations is illustrated in Figure 2(b).

2.2 The WRF Numerical Model

High-resolution regional meteorological forecasts were generated using the WRF model (version 4.1) (Stossmeister et al., 2019). A four-level nested domain configuration was employed with horizontal resolutions of 27, 9, 3, and 1 km for domains d01 to d04, respectively, as illustrated in Figure 2(a). This progressively refined grid setup enables downscaling large-scale weather patterns to a kilometer-scale resolution.

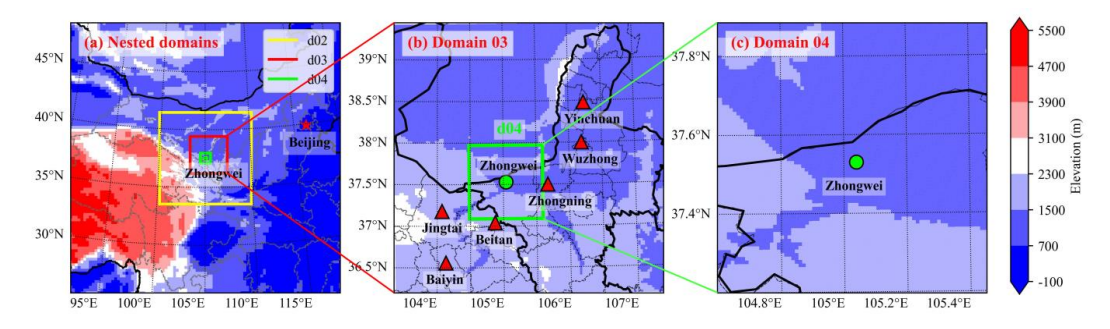


Figure 2: WRF model domain configuration and site locations. (a), Topography of the four nested WRF domains (d01-d04). (b), Map of a subregion within the d03 domain, where red markers indicate the locations of the evaluation sites. (c), A zoomed-in map of the d04 domain, with the green point marking the location of the primary observation station.

The WRF simulation period covered from 00:00 UTC on June 1, 2020, to 23:00 UTC on July 31, 2020, with hourly outputs. To emulate a realistic operational forecasting procedure, we implemented a rolling forecast scheme to create forecasts with horizons of 6, 24, 72, and 120 hours. The initial 12 hours of each simulation run were discarded as a spin-up period to ensure forecast accuracy. Consequently, the actual simulation duration was set to N+12 hours to obtain a valid N-hour forecast. Specifically, estimates of 6, 24, 72, and 120 hours corresponded to simulation durations of 18, 36, 84, and 132 hours, respectively. Each forecast cycle was initialized and bounded by the Final Operational Global Analysis data from the National Centers for Environmental Prediction (Contributor, 2015), and data assimilation was turned off across all domains. This approach not only simulates real-world forecasting practices but also reduces initial condition errors. Table S2 presents the central physics parameterization schemes used in this study. The Dudhia scheme (Dudhia, 1989), a widely adopted model in the field, was employed for shortwave radiation.

2.3 QM-TPA-LSTM Radiation Correction Model

This study proposes QM-TPA-LSTM, a hybrid post-processing model designed to correct inherent biases in NWP forecasts. The model employs a two-stage sequential correction strategy to perform rolling corrections on the GHI output from the WRF model, as illustrated in Figure 1. The QM method provides an initial statistical bias correction in the first stage. In the second stage, a TPA-LSTM network models and predicts the residual errors from the first stage. The final, refined GHI forecast is

https://doi.org/10.5194/egusphere-2025-4439 Preprint. Discussion started: 28 October 2025

© Author(s) 2025. CC BY 4.0 License.



145

150

165

EGUsphere Preprint repository

then obtained by aggregating the corrected GHI with the TPA-LSTM-predicted residuals.

QM is a highly reliable statistical method for climate bias correction (Sun et al., 2022). It performs corrections based on the statistical distributions of data rather than complex physical processes. For example, studies have shown that QM reduced WRF-simulated rainfall RMSE by 34% (Charoensuk et al., 2024), effectively minimized errors in soil moisture predictions (Koujani et al., 2025), and significantly improved precipitation and temperature forecasts (Ngai et al., 2017). The fundamental principle of QM is that for a given raw WRF forecast value, its quantile in the distribution of the raw WRF training data should be identical to the quantile of the corrected value in the distribution of the observed training data (Charoensuk et al., 2024). In this study, we employ the empirical cumulative distribution function. Although the QM correction enhances forecast accuracy, the residual errors contain valuable, yet uncaptured, predictive information. The TPA-LSTM network is employed to capture these dynamics. The TPA mechanism enhances the standard LSTM by using the final hidden state as a query to compute attention weights over all previous hidden states. A context vector is then formed as a weighted sum, allowing the model to selectively focus on historically relevant features for the current prediction, thereby improving forecast accuracy (Shih et al.,

155 2.4 PINN-iTransformer Framework

2019).

We developed the PINN-iTransformer model to achieve high-precision, multi-scale PV power forecasting by integrating physical mechanisms with an advanced deep learning architecture. This module utilizes iTransformer as its backbone network to capture complex temporal dependencies, while embedding constraints from a semi-empirical physical model via the PINN framework to enhance its generalization capability and physical interpretability.

160 2.4.1 iTransformer Model

Transformer-based architectures are widely applied in time series forecasting due to their proficiency in capturing complex temporal patterns (Piantadosi et al., 2024; Wu et al., 2024a). However, when processing multivariate time series, the conventional Transformer embeds data points from the same time step but different variables into a single token, which can weaken the correlations between variables. As shown in Figure 3, iTransformer inverts the roles of the feed-forward network and the attention mechanism within the Transformer framework. Specifically, it embeds the time points of individual series into variable-tokens, which are then processed by the attention mechanism to capture inter-variable correlations (Liu et al., 2023).



175



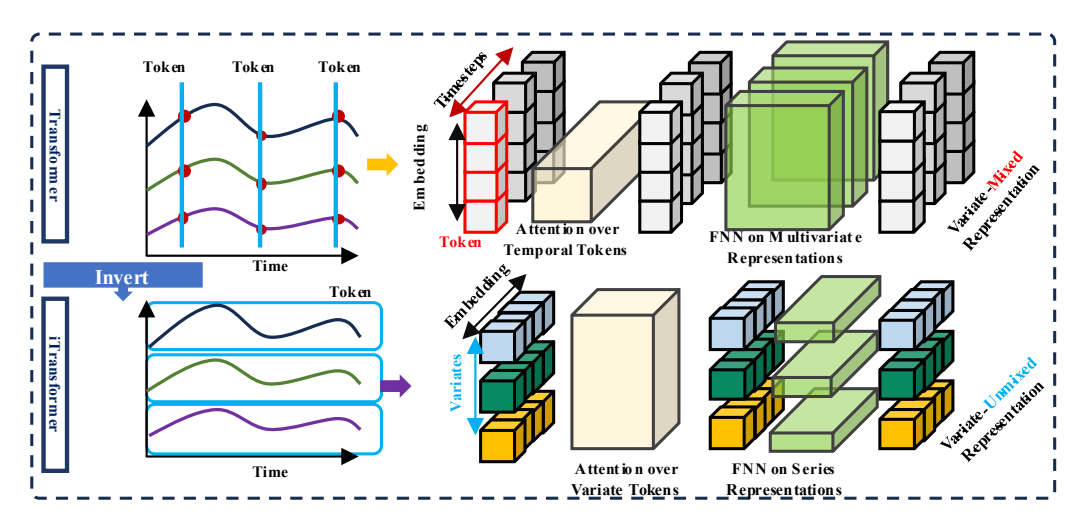


Figure 3: Schematic of the modified iTransformer architecture.

2.4.2 Physics-Informed Neural Networks

(a) Semi-empirical Physical Model

To integrate a priori physical knowledge into our data-driven framework, we employ a semi-empirical PV power model as a physical constraint. This model class was chosen for its ability to balance model complexity and predictive utility effectively. The study employs the efficient semi-empirical model proposed by Fan et al. (2025), which estimates power output based solely on solar irradiance, ambient temperature, wind speed, and a coefficient representing the thermal loss characteristics of the module. Its advantages lie in its minimal parameter requirements and high computational efficiency while retaining a description of the core physical processes.

$$P_{phy} = f_{PV} \left(\frac{G_{POA}}{G_{STC}} \right) \left[1 + \alpha_{PV} \left(T_c - T_{ref} \right) \right] P_{MPP} \tag{1}$$

$$T_c = T_a + G_{POA} expa + b \cdot \omega_s \tag{2}$$

Where, P_{phy} is the PV power output, f_{PV} represents the photovoltaic module efficiency coefficient, which is intrinsically linked to the module's manufacturing process. G_{STC} is the irradiance on the module surface under standard test conditions, α_{PV} is the photovoltaic module temperature loss coefficient, T_c is the module temperature, and T_{ref} is the module temperature under reference conditions. P_{MPP} signifies the module's maximum power, ω_s represents the wind speed, and T_a denotes the ambient temperature. The coefficients a, b are undetermined parameters that can be fitted from historical data using the least squares method.

(b) PINN Model

The core idea of PINN is to guide model training by augmenting the loss function. In addition to the standard supervised learning loss (MSE), this study introduces a physics-informed loss term. This loss term quantifies the discrepancy between the





iTransformer's output and the estimates from the semi-empirical physical model. Therefore, the total loss function is defined as a weighted sum of the supervised loss and the physics-informed loss. During model optimization, this physics-inspired regularization term compels the network to converge towards a solution space that adheres to physical laws while fitting the observational data. This prevents physically implausible predictions and significantly improves the model's dynamic consistency and extrapolation capabilities under various operating conditions. The total loss function consists of a data-driven loss and a physics-informed loss, with its mathematical formulation as follows:

$$195 \qquad \mathcal{L} = \mathcal{L}_{primary} + \lambda \mathcal{L}_{pinn} \tag{3}$$

Concurrently, a first-order ordinary differential equation (ODE) describing the dynamic temporal evolution of photovoltaic power is introduced. This equation characterizes the system's relaxation towards its equilibrium state, taking the following form:

$$\frac{d\hat{P}(t)}{dt} = -k \cdot \left(\hat{P}(t) - P_{eq}(t)\right) \tag{4}$$

Where, $\hat{P}(t)$ denotes the generated power of the module at time t, $P_{eq}(t)$ represents the theoretical equilibrium power derived from the model proposed by (Fan et al., 2025), and k is the relaxation coefficient.

The physical residual, denoted as R(t), is defined based on this ODE and can be expressed as:

$$R(t) = \frac{d\hat{P}(t)}{dt} + k \cdot (\hat{P}(t) - P_{eq}(t))$$
 (5)

Consequently, the physical loss function is formulated as the mean squared value of these residuals:

205
$$\mathcal{L}_{pinn} = \frac{1}{N} \sum_{i=1}^{N} (R_i)^2$$
 (6)

Ultimately, by minimizing the weighted total loss $\mathcal{L} = \mathcal{L}_{primary} + \lambda \mathcal{L}_{pinn}$, this work trains a model that achieves both accurate data fitting and adherence to physical principles.

3 Data Preprocessing and Feature Engineering

3.1 Reliability Analysis of NWP Output

Figure 4 presents scatter plots comparing WRF model forecasts with station observations for temperature and GHI at various lead times (6 h and 1–5 days), while Figure 5 shows a time-series comparison for GHI. The WRF model exhibits high predictive skill for temperature across all lead times, demonstrating a strong correlation with observations and low error metrics. For GHI, the model accurately reproduces the diurnal cycle and overall trends, and notably, it effectively captures sharp declines in irradiance associated with sudden weather events, such as cloud-cover changes and precipitation (indicated by the light-red shaded area in Figure 5). This capability to represent the influence of key meteorological processes on solar radiation underscores the scientific merit of the WRF forecasts. Nevertheless, a persistent systematic overestimation bias is evident in the GHI forecasts (Figure 4), with maximum errors reaching an RMSE of 231.5 W/m² and an MAE of 159.3 W/m². As solar



225



radiation is a direct input for photovoltaic power forecasting, this bias directly propagates to power predictions, introducing significant uncertainty. Consequently, bias correction of the model's radiation output is an essential step for subsequent applications (Lindsay et al., 2020).

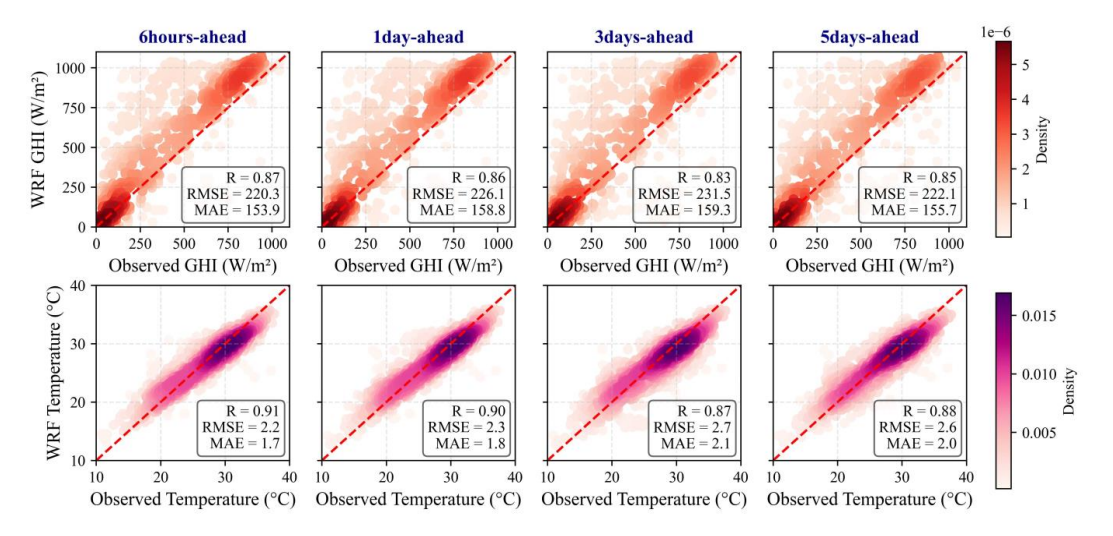


Figure 4: Comparison of WRF-simulated and observed meteorological variables at Zhongwei station.

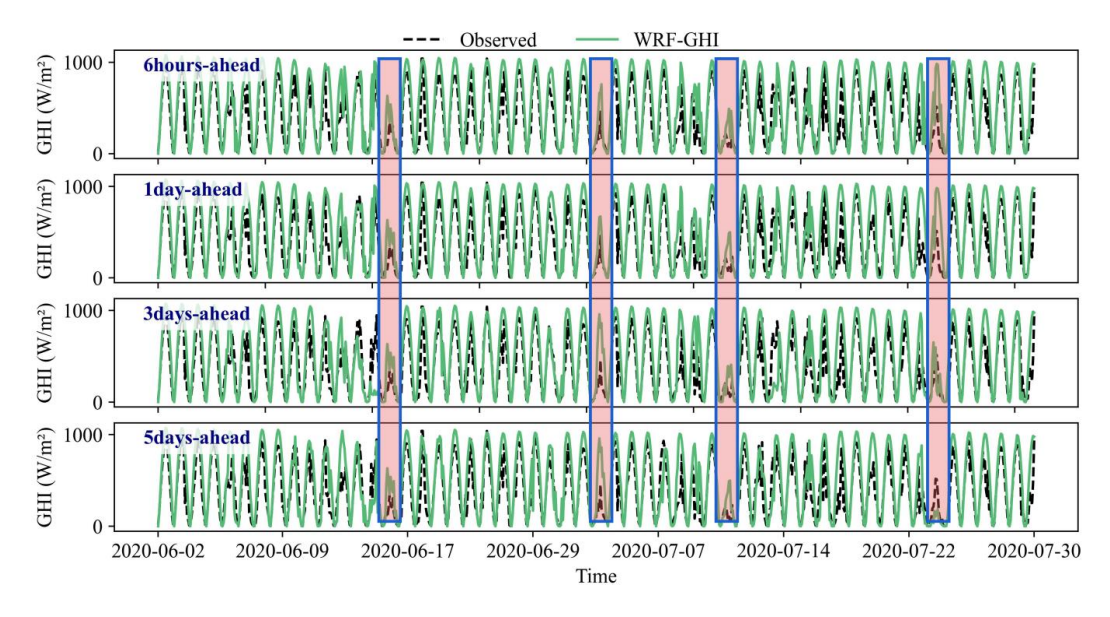


Figure 5: Time series of observed GHI versus NWP predictions at various forecast horizons.

We cross-validated the WRF model's forecasts against data from six diverse reference sites (Figure 2(b)) to rigorously assess its spatial generalizability. As illustrated in Figure 6, the WRF model's performance at these external sites is highly consistent with its performance at the local observation station, with high correlation coefficients (R). While the GHI overestimation bias persisted, its magnitude was lower than at the primary Zhongwei site. A scale mismatch likely explains this reduction. The



235

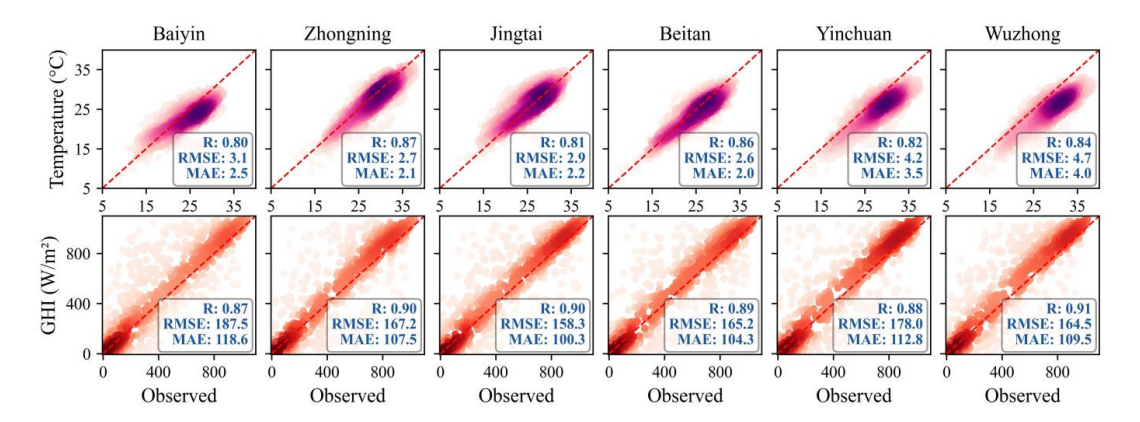
240

245

250



WRF simulation's 1 km × 1 km resolution at Zhongwei produces area-averaged irradiance, amplifying apparent GHI error compared to single ground-station point measurements. Conversely, the gridded NSRDB data provides better spatial representativeness and more closely matches the WRF output. This multi-site validation confirms that the WRF numerical model exhibits good reliability for short- to medium-range weather forecasting, providing robust environmental variable inputs for the subsequent PV power forecasting model.



This study implements real-time, multi-step rolling corrections for the WRF-derived GHI, as illustrated in the forecasting

Figure 6: Evaluation of meteorological forecasts at different sites.

3.2 GHI Correction

scheme presented in Figure 7. The framework leverages historical GHI observations and WRF meteorological parameters as inputs. During the data preprocessing phase, a dataset comprising 900 hours of valid GHI observations was constructed after cleaning and filtering. This dataset covers 60 days, with 15 daytime hours selected from each day. The dataset was partitioned into a training set (the first 400 steps), a validation set (the subsequent 100 steps), and a test set (the final 400 steps).

To simulate a realistic operational forecasting scenario, the forecast horizons were set to 6, 15 (one day ahead), 45 (three days ahead), and 75 steps (five days ahead), aligning with the WRF rolling forecast mechanism. Correspondingly, the model utilized historical data from 60, 90, 180, and 225 steps as input. This input-output length configuration is designed to capture dynamic dependencies across different time scales. An automated, non-overlapping rolling-window mechanism realizes the model's prediction process. Specifically, the model generates a GHI sequence based on historical data for a forecast horizon. After this sequence is recorded, the entire prediction window is advanced by several steps equal to the forecast horizon (e.g., after a 15-step forecast, the window slides forward 15 steps), and the next prediction begins from this new position. This process is iterated until a continuous sequence of predictions covering the entire test set is generated. The efficacy of the GHI correction at the primary Zhongwei site is illustrated in Figure 8. Its performance relative to benchmark models is detailed in Figure 9, and the generalizability of the correction is demonstrated across six additional sites in Figure 10.





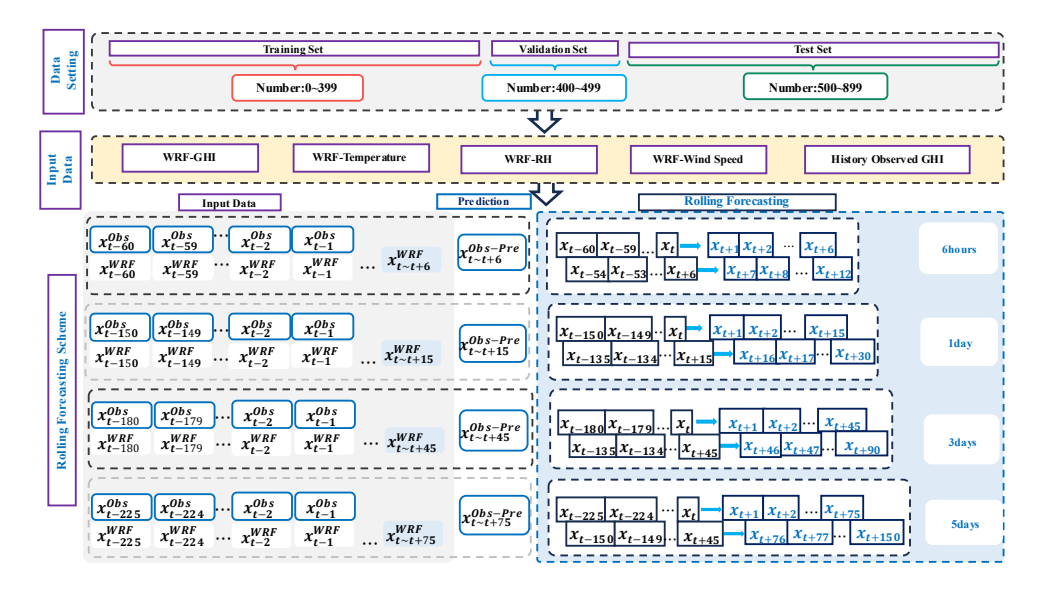


Figure 7: Schematic of the forecast output strategy. The forecast horizons are 6, 15, 45, and 75 steps, corresponding to lead times of 6 hours, 1 day, 3 days, and 5 days, respectively.

255 Figure 8 systematically illustrates the correction effect of the hybrid QM-TPA-LSTM model on the raw GHI forecasts at the Zhongwei site. The time-series plot (top) shows that the corrected GHI (blue) closely tracks the ground-truth measurements (red), effectively mitigating the substantial overestimation bias of the raw WRF forecast (green). The scatter plots on the right further corroborate this improvement from a statistical distribution perspective: the corrected data points (blue) converge more tightly around the 1:1 diagonal line (red), indicating a substantial enhancement in the consistency between predicted and observed values. The bar charts at the bottom provide a quantitative evaluation of RMSE and MAE for different forecast horizons. The results show that the corrected GHI exhibits a marked decrease in both RMSE and MAE under all conditions, with an average reduction exceeding 23%, thereby significantly improving the quality of the GHI output.

The 6-hour-ahead correction yielded the best performance, with reductions in RMSE and MAE of 33% and 36%, respectively. However, the correction performance diminishes as the forecast horizon increases. This phenomenon is likely due to two factors: (1) the inherent challenge for neural networks to model long-range temporal dependencies, and (2) a dataset size that may be insufficient for the model to learn high-frequency meteorological fluctuations.



275



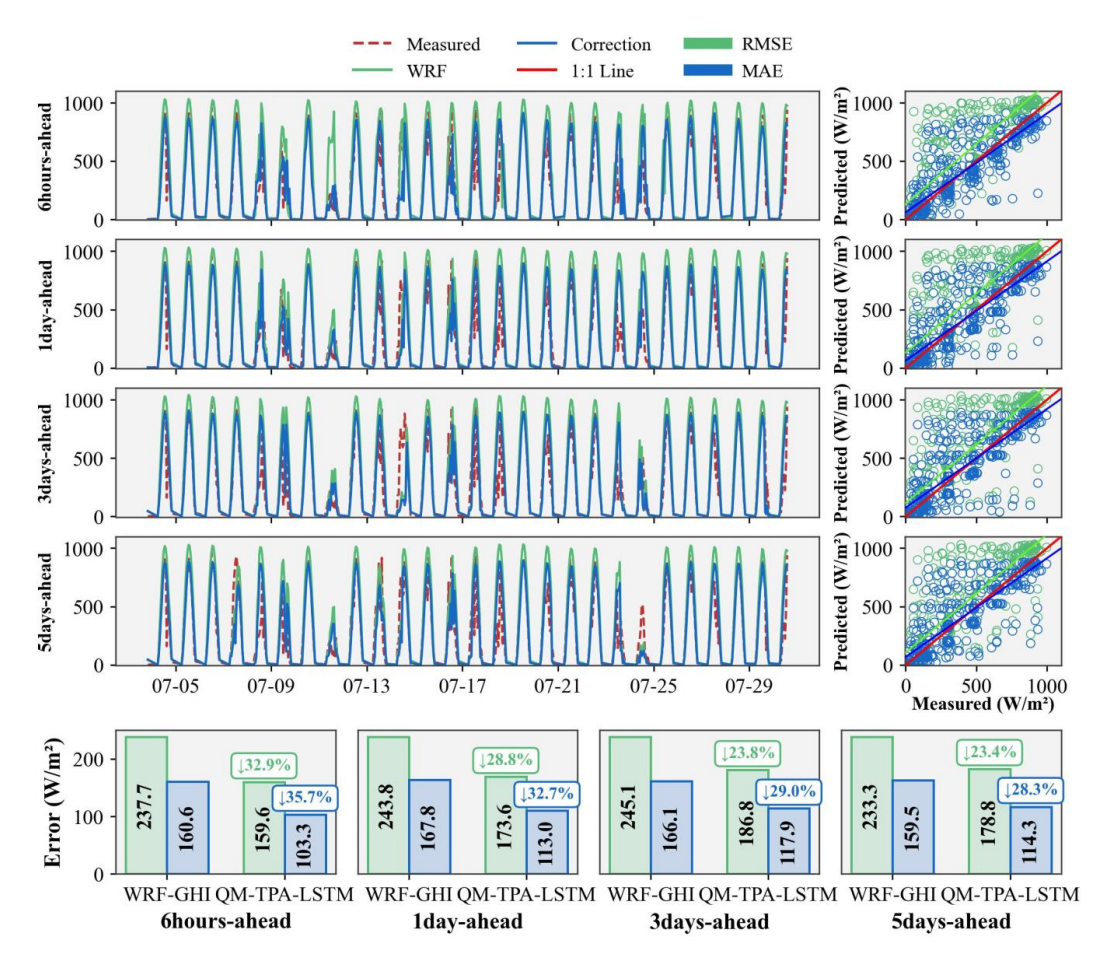


Figure 8: Performance evaluation of the GHI correction model.

The proposed QM-TPA-LSTM model was evaluated against three benchmarks across multiple forecast horizons: LSTM (Yang et al., 2025; Sun et al., 2022) and Transformer (Piantadosi et al., 2024; Wu et al., 2024a), as well as the KF model, which is widely used in meteorological correction (Visaga et al., 2024). As shown in Figure 9, all models successfully corrected the raw WRF GHI output, demonstrating the efficacy of the post-processing framework. However, the classic KF model outperformed the standard LSTM and Transformer models. This suggests that, for this specific task, standard deep learning models may not necessarily surpass established statistical methods without targeted architectural design. The proposed QM-TPA-LSTM model achieved the best correction under all conditions, with the lowest RMSE and MAE values and a distribution closer to the actual values. This validates the effectiveness of the hybrid model architecture in more effectively correcting both systematic and random errors in GHI forecasts.



285



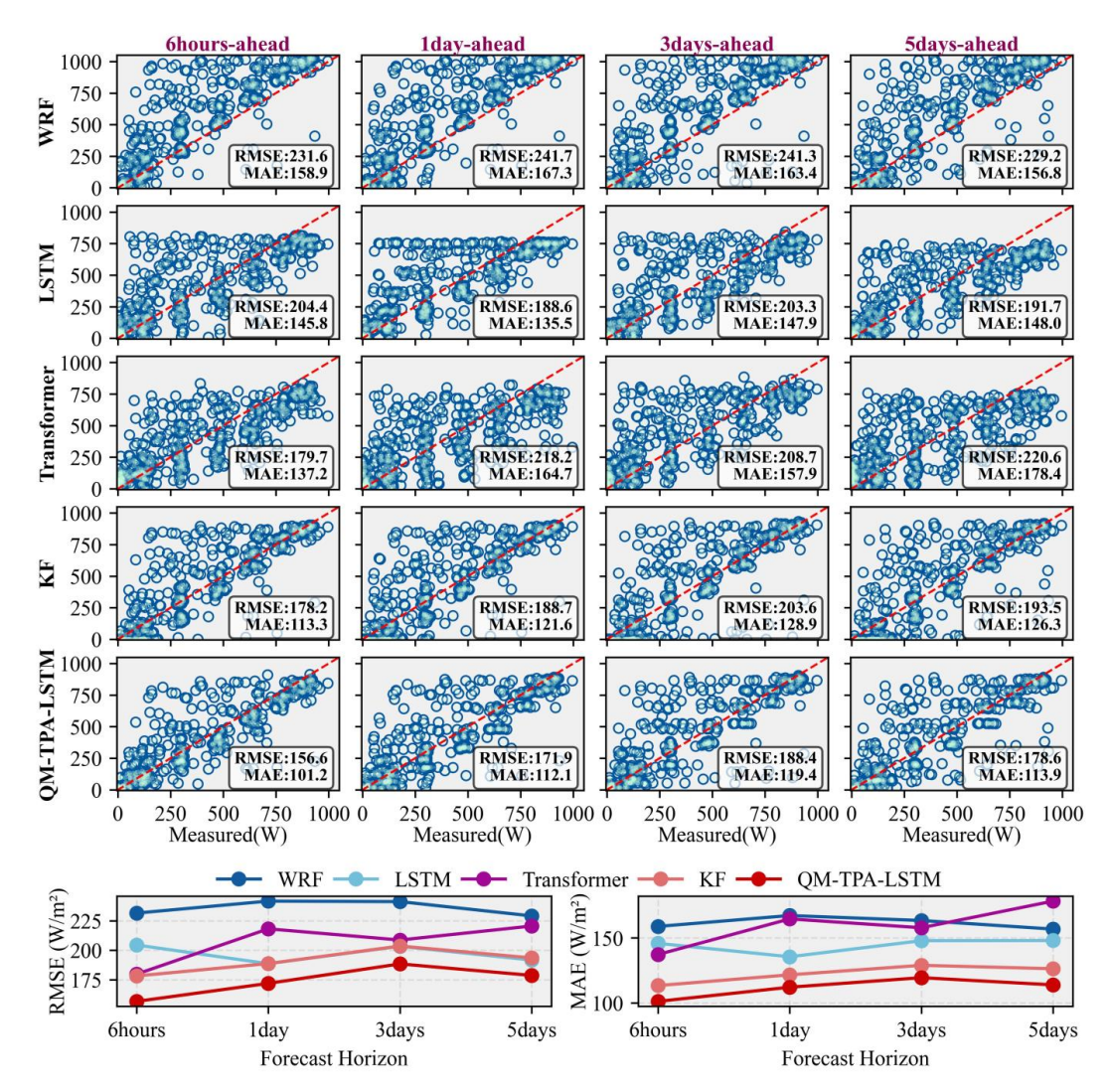


Figure 9: Comparison of different correction models for WRF-simulated GHI.

We validated the generalization of the QM-TPA-LSTM model by correcting GHI forecasts at six geographically diverse NSRDB sites. The correction results in Figure 10 show that the model consistently reduced the error of the raw WRF forecasts across all external test sites and for all forecast horizons. Specifically, the model achieved maximum reductions in RMSE and MAE of 15.1% and 17.4%, respectively, at different sites. These results provide compelling evidence that the model can effectively enhance GHI correction accuracy, even when applied to other geographical locations and data sources (e.g., NSRDB). In conclusion, our local and multi-site validations demonstrate that the proposed hybrid framework is a generalizable and effective tool for post-processing GHI in numerical weather forecasts.



295



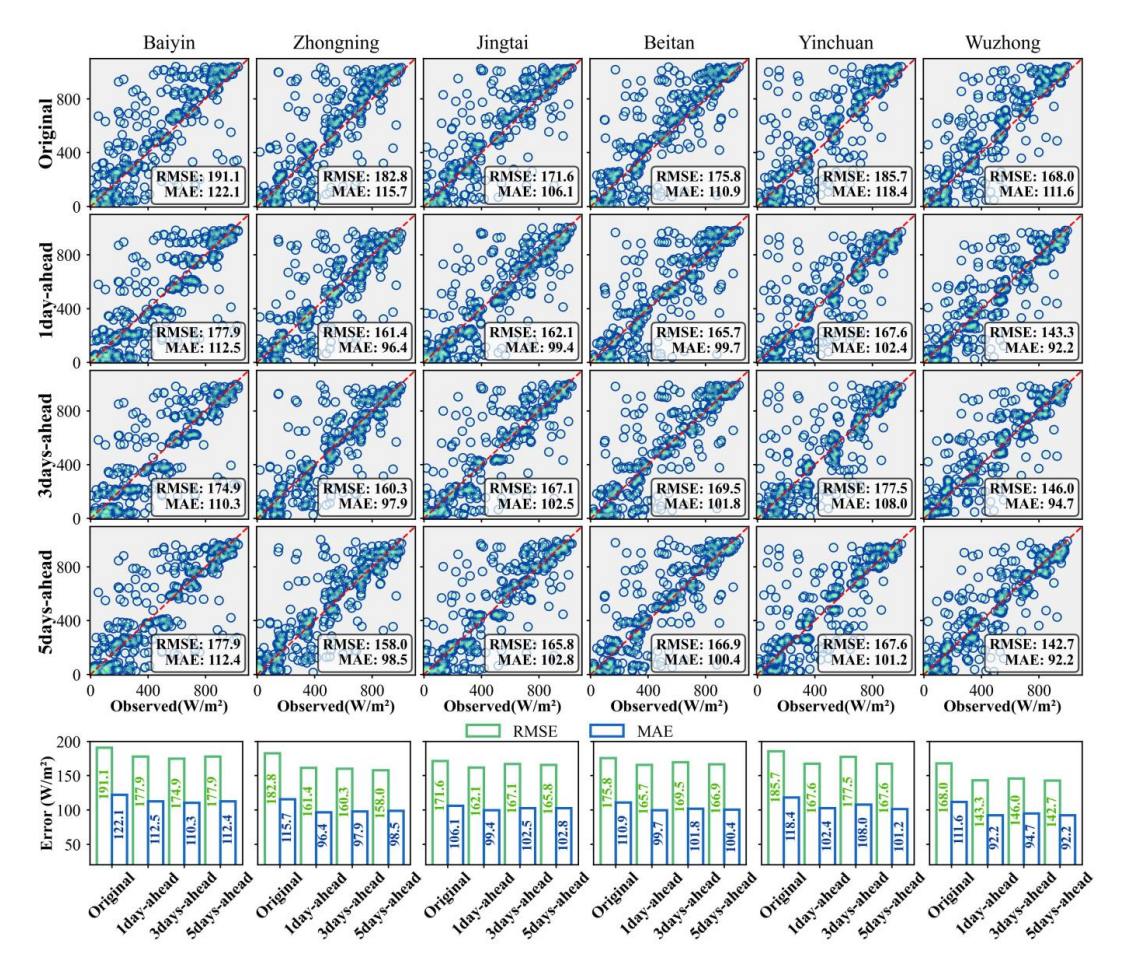


Figure 10: Evaluation of correction results using NSRDB data at multiple sites.

3.3 Calculation of Irradiance on the PV Module Surface

Although the forecast accuracy of GHI was improved through bias correction, the G_{POA} , which is the radiation actually absorbed by PV modules, is influenced by a complex interplay of multiple radiation components. Therefore, using GHI directly for power forecasting may introduce uncertainty. As shown in Figure 11(a), the instantaneous position of the sun is defined by key geometric parameters, including the solar zenith angle, solar azimuth angle, and solar elevation angle. These angles exhibit periodic, dynamic changes over time, causing significant variations in the solar irradiance received by the PV module at different moments. This variation follows a well-defined astronomical time function. Figure 11(b) further elucidates the physical composition of the irradiance received on the module surface. This total irradiance is a superposition of three components: the projection of Direct Normal Irradiance (DNI) onto the module plane, Diffuse Horizontal Irradiance (DHI), and ground-reflected irradiance (Mahmoudi et al., 2024; Anderson et al., 2023). Accurate calculation of G_{POA} requires the decomposition of GHI and the application of a radiation transposition model that incorporates the module's tilt and azimuth





angles. This is a critical step toward achieving high-precision PV power forecasting. The underlying physical principles are as follows:

$$G_{POA} = G_b + G_q + G_d \tag{7}$$

Here, G_{POA} represents the total solar irradiance on the PV module surface, G_b denotes the beam irradiance on the tilted plane, G_g is the isotropic ground-reflected irradiance, and G_d signifies the diffuse sky irradiance. The beam irradiance is

305 calculated as:

320

$$G_b = DNI \cdot cos\theta_i \tag{8}$$

Where θ_i is the angle between the sun's rays and the normal to the photovoltaic module surface (the angle of incidence). This angle can be expressed by the following equation:

$$cos\theta_i = sin\phi \cdot sin\delta \cdot cos\beta - cos\phi \cdot cos\phi \cdot cos\phi \cdot cos\omega \cdot cos\beta$$
(9)

Here, φ is the latitude of the module's location, δ is the solar declination angle, γ is the azimuth angle of the PV module, ω is the hour angle, and β is the tilt angle of the PV module installation.

The calculation principle for G_g is as follows:

$$G_g = GHI \cdot \rho \cdot \frac{(1 - \cos \beta)}{2} \tag{10}$$

The calculation principle for G_d is as follows:

$$315 G_d = DHI \cdot R_d (11)$$

Where R_d is the diffuse transposition factor.

Model for calculating G_{POA} are integrated into the pvlib-python library developed by Sandia National Laboratories (Anderson et al., 2023). In this study, we first employed the Erbs model to decompose GHI (Erbs et al., 1982). Subsequently, the classic Hay-Davies anisotropic sky model was used to calculate the diffuse irradiance received on the tilted surface of the PV module (Hay, 1979). The ground-reflected irradiance component was estimated based on a constant ground albedo of 0.2, a typical value for common vegetation or soil surfaces. In Figure 11(c), the blue curve represents the corrected GHI time series, while the red curve shows the resulting G_{POA} time series.

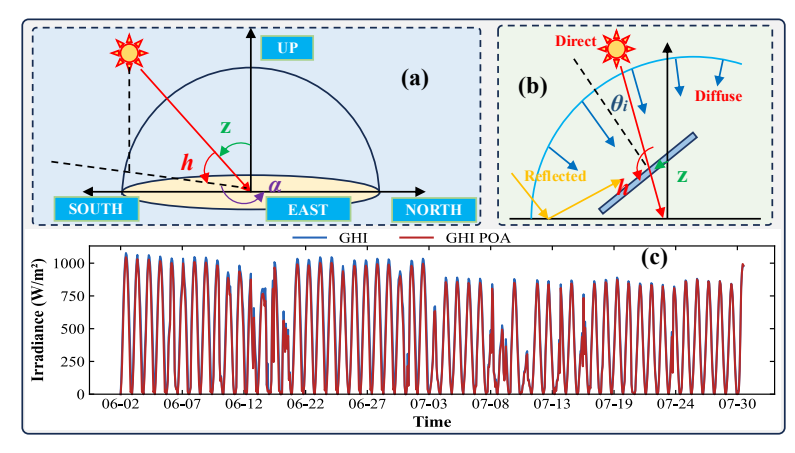


Figure 11: Solar geometry and irradiance components. (a), Schematic illustrating the solar zenith, azimuth, and altitude angles. (b),



335



325 Components of solar irradiance on a tilted PV module surface. (c), Time series of the corrected GHI and the calculated G_{PQA} .

4 PV Power Forecasting and Evaluation

A comparative study was designed to validate the PINN-iTransformer using operational data from a station in Zhongwei. The overall forecasting architecture is depicted in Figure 12. The experimental protocol involved partitioning the dataset into training (80%), validation (10%), and testing (10%) sets to prevent information leakage. We benchmarked our proposed PINN-iTransformer against a suite of models representing distinct strategies for integrating physical principles with deep learning. The comparison began with a standard iTransformer, a purely data-driven baseline. We then evaluated a tandem hybrid model (Physics-iTransformer), where an initial forecast from a physical model is corrected by a subsequent iTransformer that learns the residual error. Finally, we assessed a physics-constrained model (PC-iTransformer), which incorporates a physical model from (Fan et al., 2025) as a soft constraint by penalizing deviations from physical laws within the loss function. Performance was systematically evaluated across multiple forecast horizons: 6 hours, 1 day, 3 days, and 5 days. Figures 13-15 demonstrate that the PINN-iTransformer architecture consistently outperformed all competing models, confirming its superior predictive accuracy.

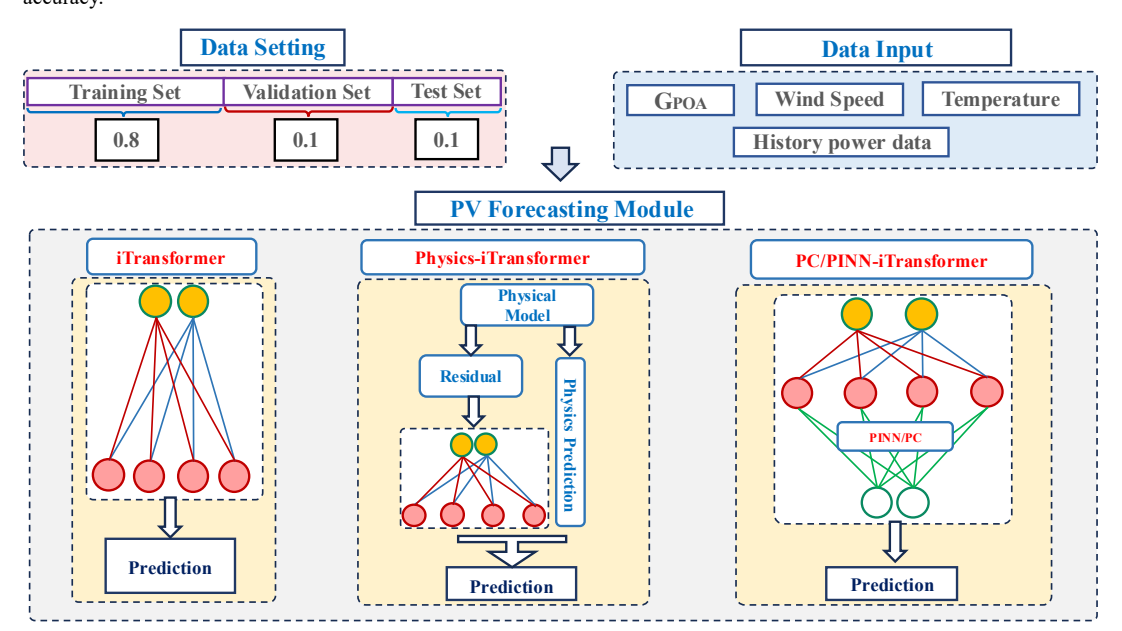


Figure 12: Schematic of the PV power forecasting framework.

Figure 13 presents a comprehensive performance evaluation of the four primary forecasting models across multiple horizons.

The analysis reveals a clear hierarchy of performance. The serial hybrid model (Physics-iTransformer) exhibited the poorest performance, with its error metrics (R, MAE, RMSE) significantly higher than those of other models. This suggests a simple residual correction framework is prone to error accumulation and amplification. The purely data-driven iTransformer occasionally generated physically implausible negative power values, a common artifact of deep learning models lacking



355

360



physical boundary constraints. In stark contrast, models incorporating physical knowledge demonstrated markedly superior reliability. Both the PC-iTransformer and our proposed PINN-iTransformer outperformed the baseline models. Notably, the PINN-iTransformer achieved the best overall performance, consistently yielding the highest R and the lowest MAE and RMSE across all forecast horizons. This result supports the hypothesis that integrating physical differential equations deeply into the network architecture, as the PINN framework does, substantially enhances model generalization and predictive accuracy.

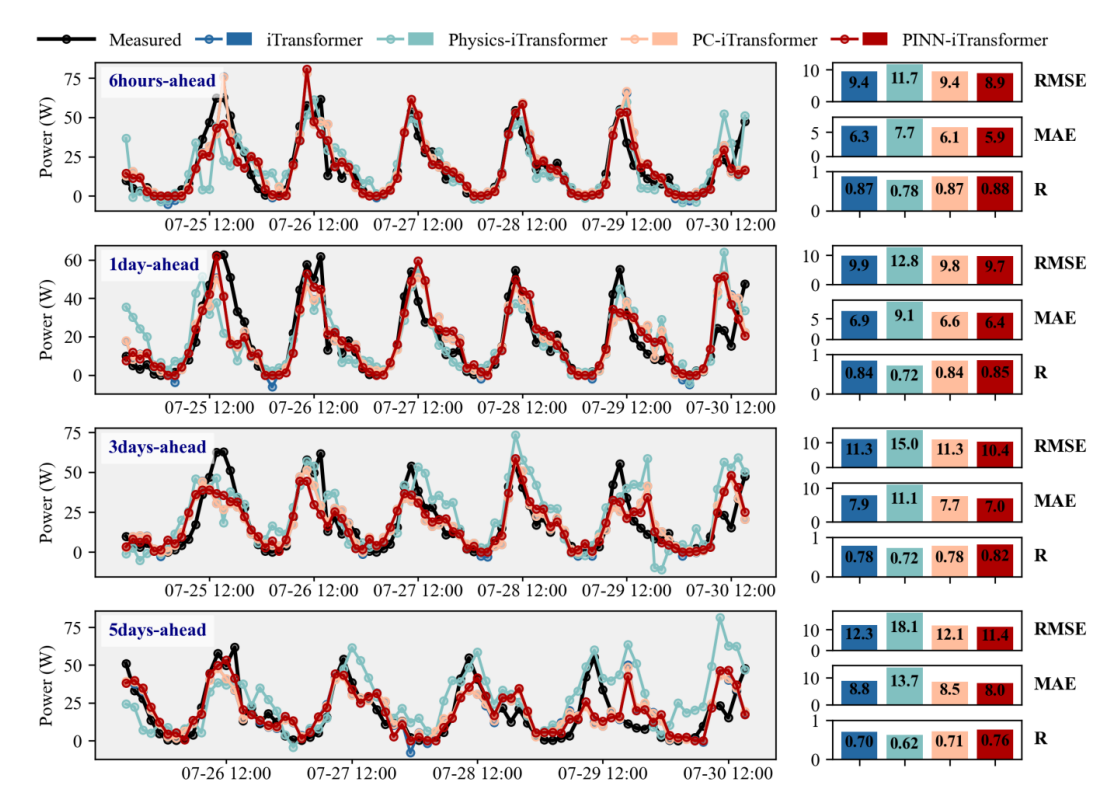


Figure 13: Time series plot of PV power predictions and error histogram evaluation.

The predictive accuracy of all models degrades over longer forecast horizons, a deterioration attributable to three factors. First, cumulative error in the WRF-derived GHI propagates through the forecast, directly impairing power prediction. Second, the capacity of neural networks to maintain long-term temporal dependencies inherently diminishes across extended sequences. Finally, the limited training dataset constrains the model's ability to learn features robust enough for long-range inference, amplifying prediction errors.

Furthermore, to better reflect real-world engineering applications and address the computational cost of WRF simulations, specifically, the resource redundancy from short rolling steps needed to avoid 'spin-up' errors, we used a 5-day rolling WRF forecast to evaluate performance. As shown in Figure 14, the PINN-iTransformer model's predictions align more closely with the 1:1 line than the benchmarks. Across all forecast horizons, the model consistently outperforms all benchmark models,





reducing RMSE and MAE by up to 15.5% and 12.44%, respectively. Notably, while prediction errors for all models increase with the forecast horizon, the PINN-iTransformer maintains the lowest RMSE and MAE.

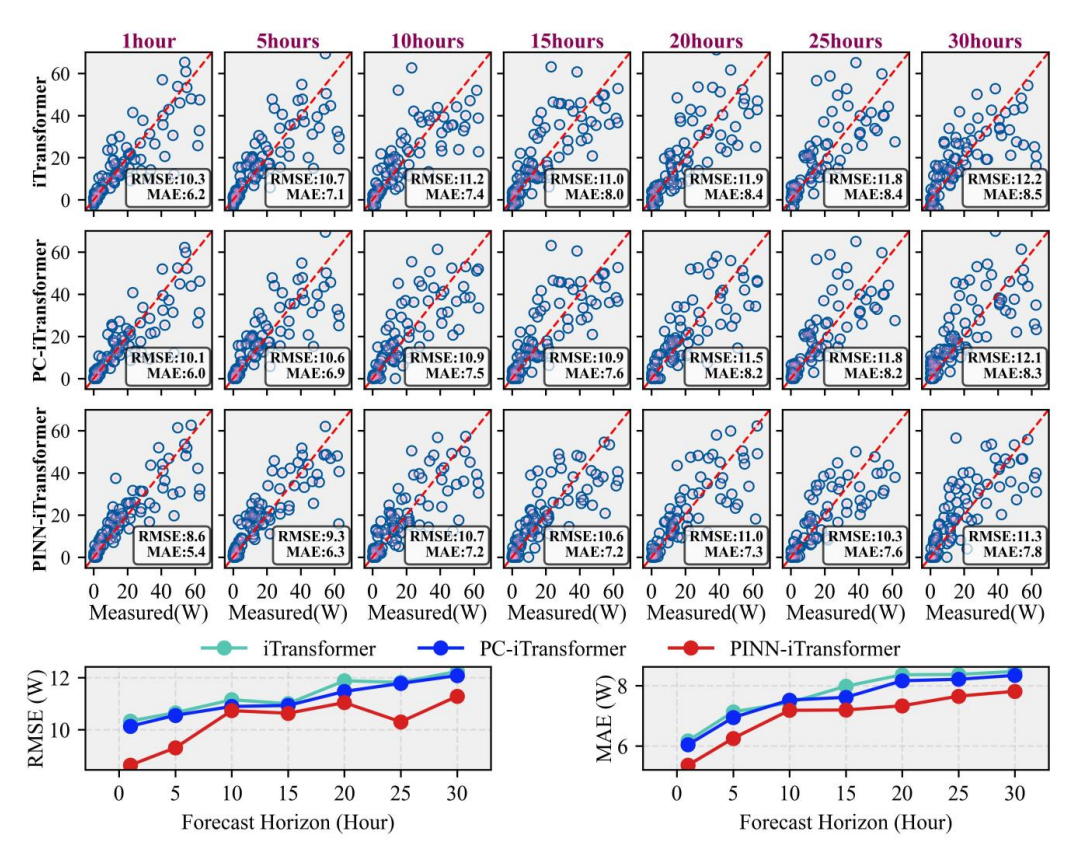


Figure 14: Multi-step PV power forecasting performance using a 5-day WRF forecast.

The proposed PINN-iTransformer was evaluated against a diverse set of benchmarks, including LSTM (Yang et al., 2025), the 365 frequency-domain-based TimsNet (Yu et al., 2025), a hybrid model integrating an attention mechanism, CNN-Attention-BiGRU (Dai et al., 2024), and the multilayer perceptron-based TSMixer (Ekambaram et al., 2023). All models were evaluated using the same multi-step forecasting tasks. The results, presented in Figure 15, clearly demonstrate the outstanding performance of the PINN-iTransformer. Its RMSE and MAE metrics are significantly lower for all specified forecast horizons than for all benchmark models.

370





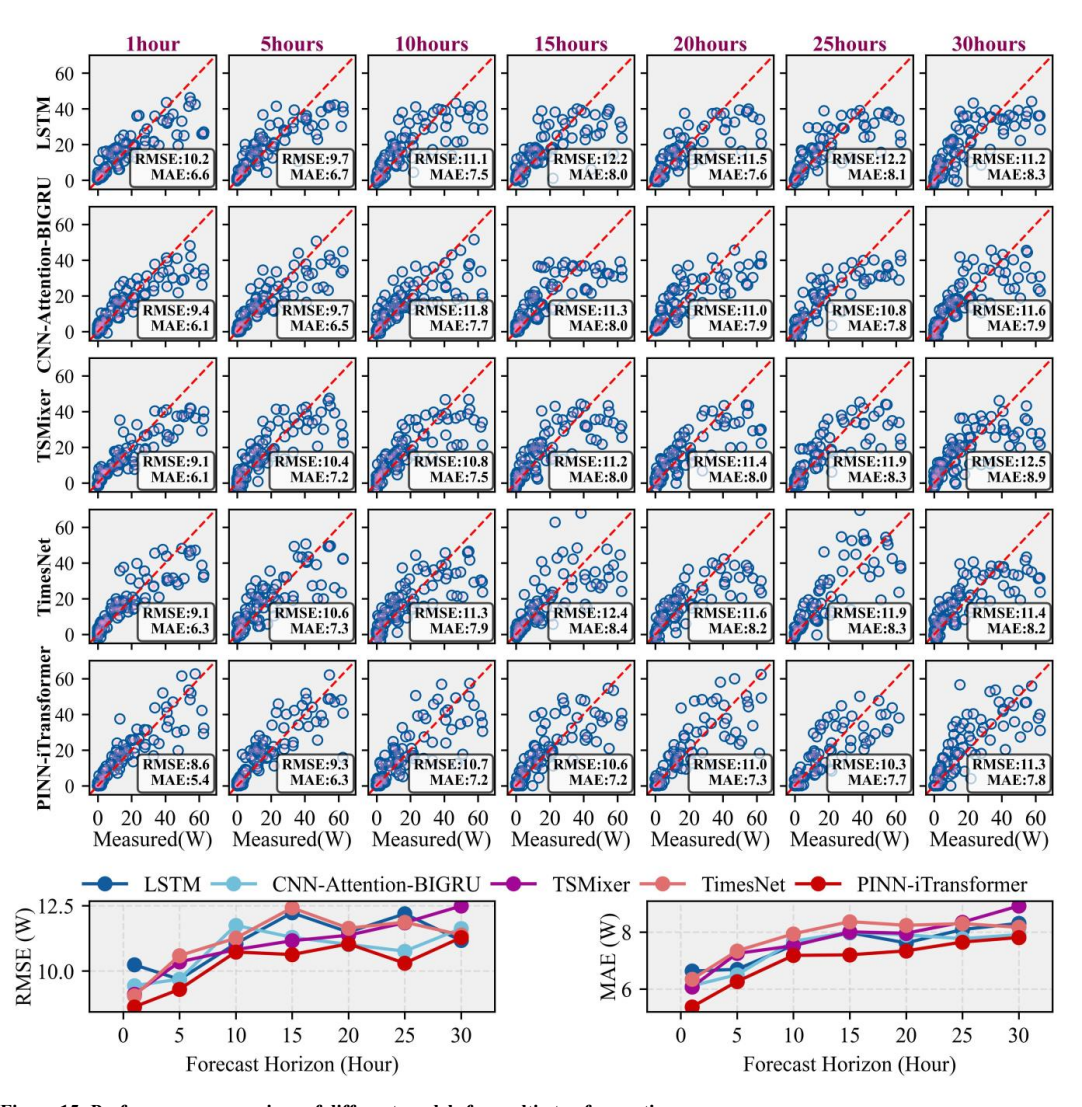


Figure 15: Performance comparison of different models for multi-step forecasting.

5 Conclusion

380

This study proposes a physics-informed real-time forecasting framework (MIPV-NWP-PINN) designed to overcome key limitations—such as poor generalizability and physical inconsistency—in conventional data-driven approaches for photovoltaic (PV) power forecasting. The framework establishes an end-to-end prediction pipeline that integrates high-resolution numerical weather prediction (NWP), a novel global horizontal irradiance (GHI) bias correction model, and a physics-constrained deep learning architecture.

First, the hybrid QM-TPA-LSTM model synergistically combines statistical quantile mapping with deep temporal pattern

https://doi.org/10.5194/egusphere-2025-4439 Preprint. Discussion started: 28 October 2025





385

390

395

400

405

EGUsphere Preprint repository

extraction, achieving superior GHI bias correction accuracy across forecasting horizons ranging from 6 hours to 5 days,

outperforming existing methods including standalone neural networks and Kalman filter (KF) models.

Second, the newly developed PINN-iTransformer architecture for power forecasting explicitly incorporates physical principles

into the network design. This integration ensures physically plausible predictions, effectively guiding the learning process and

substantially improving model generalization and stability. As a result, the PINN-iTransformer consistently exceeded the

performance of state-of-the-art time-series models across all evaluated forecast horizons.

While this study demonstrates a robust proof of concept at a single station, future work will focus on validating and extending

the framework's applicability across diverse geographical and climatic conditions. Additionally, although the GHI correction

component proves effective, it remains largely data-driven. A critical direction for future research is to enhance its physical

fidelity through explicit modeling of radiative transfer effects influenced by atmospheric constituents such as clouds,

anthropogenic aerosols, and dust.

Code and data availability. The observed data, geospatial data, WRF simulated data and all code can be found on Zenodo

(https://doi.org/10.5281/zenodo.17086317, Zhang et al. (2025)).

Interactive computing environment. The computational experiments were conducted using Python version 3.10 in a

TensorFlow environment.

Author contributions. Fei Zhang developed the model and wrote the paper with suggestions from all co-authors. Xingcai Li

provided the critical observed data, designed the method, and edited the paper. Xueshun Chen conceived the idea, supported

the coding, and edited the paper. Xueshun Chen and Zifa Wang provided scientific guidance throughout all research advances.

Yunyun Wen offered the plot code. Xuyang Zhou, Zichen Wu, and Zhuoran Wang offered analysis and polished the paper.

Huansheng Chen and Zhe Wang provided technical support and edited the paper.

Competing interests. The contact author has declared that none of the authors has any competing interests.

Acknowledgements. The authors extend their heartfelt appreciation to NECP for providing the climate reanalysis product

and TensorFlow for offering the sophisticated machine learning library that served as the cornerstone for conducting

these experiments. We thank for the technical support of the National Large Scientific and Technological Infrastructure "Earth

System Numerical Simulation Facility" (https://cstr.cn/31134.02.EL). We also thank the editors and reviewers for providing

constructive comments and suggestions to help us improve the manuscript.

Financial support. This work is supported by the National Natural Science Foundation of China (grant no. 12064034,

20





42377105), the Excellent Youth Project of Ningxia Natural Science Foundation (2024AAC05040) and the Leading Talents

410 Program of Science and Technology innovation in Ningxia Province (2020GKLRLX08).

Reference

- Alvarenga, R., Herbaux, H., and Linguet, L.: Combination of Post-Processing Methods to Improve High-Resolution NWP Solar Irradiance Forecasts in French Guiana, 10.3390/engproc2022018027, 2022.
- Anderson, K., Hansen, C., Holmgren, W., Jensen, A., Mikofski, M., and Driesse, A.: pvlib python: 2023 project update, Journal of Open Source Software, 8, 5994, 10.21105/joss.05994, 2023.
 Charoensuk, T., Luchner, J., Balbarini, N., Sisomphon, P., and Bauer-Gottwein, P.: Enhancing the capabilities of the Chao Phraya forecasting system through the integration of pre-processed numerical weather forecasts, Journal of Hydrology: Regional Studies, 52, 101737, https://doi.org/10.1016/j.ejrh.2024.101737, 2024.
- 420 contributor: NCEP GDAS/FNL 0.25 Degree Global Tropospheric Analyses and Forecast Grids, Research Data Archive at the National Center for Atmospheric Research, Computational and Information Systems Laboratory [dataset], 2015.
 Dai, H., Zhen, Z., Wang, F., Lin, Y., Xu, F., and Duić, N.: A short-term PV power forecasting method based on weather type credibility prediction and multi-model dynamic combination, Energy Conversion and Management, 326, 119501, https://doi.org/10.1016/j.enconman.2025.119501, 2025.
- Dai, Y., Yu, W., and Leng, M.: A hybrid ensemble optimized BiGRU method for short-term photovoltaic generation forecasting, Energy, 299, 131458, https://doi.org/10.1016/j.energy.2024.131458, 2024.
 Das, U. K., Tey, K. S., Seyedmahmoudian, M., Mekhilef, S., Idris, M. Y. I., Van Deventer, W., Horan, B., and Stojcevski, A.: Forecasting of photovoltaic power generation and model optimization: A review, Renewable and Sustainable Energy Reviews, 81, 912-928, https://doi.org/10.1016/j.rser.2017.08.017, 2018.
- De Soto, W., Klein, S. A., and Beckman, W. A.: Improvement and validation of a model for photovoltaic array performance, Solar Energy, 80, 78-88, https://doi.org/10.1016/j.solener.2005.06.010, 2006.
 Dolara, A., Grimaccia, F., Leva, S., Mussetta, M., and Ogliari, E.: A Physical Hybrid Artificial Neural Network for Short Term Forecasting of PV Plant Power Output, 10.3390/en8021138, 2015.
 Dudhia, J.: Numerical Study of Convection Observed during the Winter Monsoon Experiment Using a Mesoscale Two-
- Dimensional Model, Journal of Atmospheric Sciences, 46, 3077-3107, https://doi.org/10.1175/1520-0469(1989)046
 Ekambaram, V., Jati, A., Nguyen, N., Sinthong, P., and Kalagnanam, J.: TSMixer: Lightweight MLP-Mixer Model for Multivariate Time Series Forecasting, Proceedings of the 29th ACM SIGKDD Conference on Knowledge Discovery and Data
- Multivariate Time Series Forecasting, Proceedings of the 29th ACM SIGKDD Conference on Knowledge Discovery and Data Mining, Long Beach, CA, USA, 10.1145/3580305.3599533, 2023.
 Erbs, D. G., Klein, S. A., and Duffie, J. A.: Estimation of the diffuse radiation fraction for hourly, daily and monthly-average
- global radiation, Solar Energy, 28, 293-302, https://doi.org/10.1016/0038-092X(82)90302-4, 1982.

 Fan, S., Geng, H., Zhang, H., Yang, J., and Hiroichi, K.: Photovoltaic power forecasting model employing epoch-dependent adaptive loss weighting and data assimilation, Solar Energy, 290, 113351, https://doi.org/10.1016/j.solener.2025.113351, 2025.

 Guo, F., Yang, C., Xia, D., and Xu, J.: Short-Term Prediction of Photovoltaic Power Based on Improved CNN-LSTM and
- Cascading Learning, Energy Engineering, 122, 1975-1999, https://doi.org/10.32604/ee.2025.062035, 2025.
 Gupta, M., Arya, A., Varshney, U., Mittal, J., and Tomar, A.: A review of PV power forecasting using machine learning techniques, Progress in Engineering Science, 2, 100058, https://doi.org/10.1016/j.pes.2025.100058, 2025.
 Hay, J. E.: Calculation of monthly mean solar radiation for horizontal and inclined surfaces, Solar Energy, 23, 301-307, https://doi.org/10.1016/0038-092X(79)90123-3, 1979.
- Hottel, H. C.: A simple model for estimating the transmittance of direct solar radiation through clear atmospheres, Solar Energy, 18, 129-134, https://doi.org/10.1016/0038-092X(76)90045-1, 1976.



495



- IEA: Share of renewable electricity generation by technology, 2024.
- Khan, M. U. and Jama, M. A.: Evaluation and correction of solar irradiance in Somaliland using ground measurements and global reanalysis products, Heliyon, 10, e35256, https://doi.org/10.1016/j.heliyon.2024.e35256, 2024.
- Koujani, S. R., Hosseini, S. A., and Sharafati, A.: Soil moisture downscaling in the state of Oklahoma: Employing advanced machine learning, Journal of Atmospheric and Solar-Terrestrial Physics, 268, 106454, https://doi.org/10.1016/j.jastp.2025.106454, 2025.
 - Li, C., Xu, Y., Xie, M., Zhang, P., Zhang, B., Xiao, B., Zhang, S., Liu, Z., Zhang, W., and Hao, X.: Assessing solar-to-PV power conversion models: Physical, ML, and hybrid approaches across diverse scales, Energy, 323, 135744, https://doi.org/10.1016/j.energy.2025.135744, 2025.
 - Lindsay, N., Libois, Q., Badosa, J., Migan-Dubois, A., and Bourdin, V.: Errors in PV power modelling due to the lack of spectral and angular details of solar irradiance inputs, Solar Energy, 197, 266-278, https://doi.org/10.1016/j.solener.2019.12.042, 2020.
- Liu, P., Quan, F., Gao, Y., Alotaibi, B., Alsenani, T. R., and Abuhussain, M.: Green energy forecasting using multiheaded convolutional LSTM model for sustainable life, Sustainable Energy Technologies and Assessments, 63, 103609, https://doi.org/10.1016/j.seta.2024.103609, 2024.
 - Liu, W. and Gai, M.: PV-MLP: A lightweight patch-based multi-layer perceptron network with time—frequency domain fusion for accurate long-sequence photovoltaic power forecasting, Renewable Energy, 251, 123277, https://doi.org/10.1016/j.renene.2025.123277, 2025.
- Liu, Y., Hu, T., Zhang, H., Wu, H., Wang, S., Ma, L., and Long, M.: itransformer: Inverted transformers are effective for time series forecasting, arXiv preprint arXiv:2310.06625, 2023.
 - Mahmoudi, E., de Souza Silva, J. L., and dos Santos Barros, T. A.: Assessing the performance of physical transposition models in photovoltaic power forecasting: A comprehensive micro and macro accuracy analysis, Energy Conversion and Management: X, 24, 100792, https://doi.org/10.1016/j.ecmx.2024.100792, 2024.
- Ngai, S. T., Tangang, F., and Juneng, L.: Bias correction of global and regional simulated daily precipitation and surface mean temperature over Southeast Asia using quantile mapping method, Global and Planetary Change, 149, 79-90, https://doi.org/10.1016/j.gloplacha.2016.12.009, 2017.
 - Nie, X. and Mao, Q.: Study on shortwave radiative transfer characteristics in polydisperse aerosols in a clear sky, Infrared Physics & Technology, 118, 103903, https://doi.org/10.1016/j.infrared.2021.103903, 2021.
- Peng, S., Zhu, J., Wu, T., Yuan, C., Cang, J., Zhang, K., and Pecht, M.: Prediction of wind and PV power by fusing the multi-stage feature extraction and a PSO-BiLSTM model, Energy, 298, 131345, https://doi.org/10.1016/j.energy.2024.131345, 2024.
 Piantadosi, G., Dutto, S., Galli, A., De Vito, S., Sansone, C., and Di Francia, G.: Photovoltaic power forecasting: A Transformer based framework, Energy and AI, 18, 100444, https://doi.org/10.1016/j.egyai.2024.100444, 2024.
- Raissi, M., Perdikaris, P., and Karniadakis, G. E.: Physics-informed neural networks: A deep learning framework for solving forward and inverse problems involving nonlinear partial differential equations, Journal of Computational Physics, 378, 686-707, https://doi.org/10.1016/j.jcp.2018.10.045, 2019.
 - Rincón, A., Jorba, O., Frutos, M., Alvarez, L., Barrios, F. P., and González, J. A.: Bias correction of global irradiance modelled with weather and research forecasting model over Paraguay, Solar Energy, 170, 201-211, https://doi.org/10.1016/j.solener.2018.05.061, 2018.
- 490 Ruiz-Arias, J. A., Dudhia, J., and Gueymard, C. A.: A simple parameterization of the short-wave aerosol optical properties for surface direct and diffuse irradiances assessment in a numerical weather model, Geosci. Model Dev., 7, 1159-1174, 10.5194/gmd-7-1159-2014, 2014.
 - Santos, L. d. O., AlSkaif, T., Barroso, G. C., and Carvalho, P. C. M. d.: Photovoltaic power estimation and forecast models integrating physics and machine learning: A review on hybrid techniques, Solar Energy, 284, 113044, https://doi.org/10.1016/j.solener.2024.113044, 2024.
 - Sengupta, M., Xie, Y., Lopez, A., Habte, A., Maclaurin, G., and Shelby, J.: The National Solar Radiation Data Base (NSRDB), Renewable and Sustainable Energy Reviews, 89, 51-60, https://doi.org/10.1016/j.rser.2018.03.003, 2018.
 - Shih, S.-Y., Sun, F.-K., and Lee, H.-y.: Temporal pattern attention for multivariate time series forecasting, Machine Learning,





108, 1421-1441, 10.1007/s10994-019-05815-0, 2019.

https://doi.org/10.1016/j.renene.2015.08.057, 2016.

- Stossmeister, G. J., Gill, D. O., Powers, J. G., and Duda, M. G.: A Description of the Advanced Research WRF Model Version 4.1, A Description of the Advanced Research WRF Model Version 4.1 (2019) NCAR/TN-556+STR, 556, 10.5065/1dfh-6p97, 2019.
 - Sun, H., Fung, J. C. H., Chen, Y., Li, Z., Yuan, D., Chen, W., and Lu, X.: Development of an LSTM broadcasting deep-learning framework for regional air pollution forecast improvement, Geosci. Model Dev., 15, 8439-8452, 10.5194/gmd-15-8439-2022,
 - Visaga, S. M., Pascua, P. J., Tonga, L. P., Olaguera, L. M., Cruz, F. A., Alvarenga, R., Bucholtz, A., Magnaye, A. M., Simpas, J. B., Reid, E., Uy, S. N., and Villarin, J. R.: Application of Kalman filter for post-processing WRF-Solar forecasts over Metro Manila, Philippines, Solar Energy, 283, 113050, https://doi.org/10.1016/j.solener.2024.113050, 2024.
- Vu, B. H. and Chung, I.-Y.: Optimal generation scheduling and operating reserve management for PV generation using RNN-510 based forecasting models for stand-alone microgrids, Renewable Energy, 195, 1137-1154, https://doi.org/10.1016/j.renene.2022.06.086, 2022.
 - Wang, K., Qi, X., and Liu, H.: A comparison of day-ahead photovoltaic power forecasting models based on deep learning neural network, Applied Energy, 251, 113315, https://doi.org/10.1016/j.apenergy.2019.113315, 2019.
- Wu, J., Zhao, Y., Zhang, R., Li, X., and Wu, Y.: Application of three Transformer neural networks for short-term photovoltaic power prediction: A case study, Solar Compass, 12, 100089, https://doi.org/10.1016/j.solcom.2024.100089, 2024a.
 - Wu, Y., Liu, J., Li, S., and Jin, M.: Physical model and long short-term memory-based combined prediction of photovoltaic power generation, Journal of Power Electronics, 24, 1118-1128, 10.1007/s43236-024-00782-9, 2024b.
 - Yang, F., Fu, X., and Zhang, Y.: 2 LSTM-based day-ahead photovoltaic power prediction, in: Statistical Relational Artificial Intelligence in Photovoltaic Power Uncertainty Analysis, edited by: Fu, X., Elsevier, 35-70, https://doi.org/10.1016/B978-0-443-34041-3.00009-2, 2025.
- 520 443-34041-3.00009-2, 2025.

 Yu, S., He, B., and Fang, L.: Multi-step short-term forecasting of photovoltaic power utilizing TimesNet with enhanced feature extraction and a novel loss function, Applied Energy, 388, 125645, https://doi.org/10.1016/j.apenergy.2025.125645, 2025.

 Yue, X., Tang, X., Hu, B., Chen, K., Wu, Q., Kong, L., Wu, H., Wang, Z., and Zhu, J.: Evaluation of the simulation performance of WRF-Solar for a summer month in China using ground observation network data, Atmospheric and Oceanic Science Letters,
- 525 18, 100532, https://doi.org/10.1016/j.aosl.2024.100532, 2025.

 Zempila, M.-M., Giannaros, T. M., Bais, A., Melas, D., and Kazantzidis, A.: Evaluation of WRF shortwave radiation parameterizations in predicting Global Horizontal Irradiance in Greece, Renewable Energy, 86, 831-840,
- Zhai, C., He, X., Cao, Z., Abdou-Tankari, M., Wang, Y., and Zhang, M.: Photovoltaic power forecasting based on VMD-SSA-530 Transformer: Multidimensional analysis of dataset length, weather mutation and forecast accuracy, Energy, 324, 135971, https://doi.org/10.1016/j.energy.2025.135971, 2025.
 - Zhang, F., Li, X., and Chen, X.: Development of a Multi-scale Photovoltaic Power Forecasting Framework Integrating Numerical Weather Prediction with Physics-Informed Neural Networks, Zenodo [dataset], https://doi.org/10.5281/zenodo.17086317, 2025.
- Zhang, X., Li, Y., Li, T., Gui, Y., Sun, Q., and Gao, D. W.: Digital Twin Empowered PV Power Prediction, Journal of Modern Power Systems and Clean Energy, 12, 1472-1483, 10.35833/MPCE.2023.000351, 2024.